JOURNAL OF MATERIALS SCIENCE 10 (1975) 2156–2170

Review
The design of single crystal materials for magnetic bubble domain applications

J. E. DAVIES, E. A. GIESS
IBM Thomas J. Watson Research Center, Yorktown Heights, New York, USA

The criteria for the existence of stable magnetic bubble domains and their potential in data storage applications are outlined. The development of single crystal materials capable of supporting such domains is reviewed. Particular emphasis is given to both the static and dynamic properties of bubble domains and to how, by careful materials design and preparation, the optimum balance of these properties can be attained.

1. Introduction

The concept of magnetic domains was originated at the turn of this century by Weiss [1] and has become one of the most important principles in magnetism. During 1967, Bobeck [2] proposed that small cylindrical magnetic domains (the so-called magnetic bubbles), supported in thin single crystal platelets, could be manipulated to provide a method of data storage. The relative merits of a magnetic bubble memory have been discussed and compared with conventional data storage methods by Bobeck and Scovil [3]. In short, magnetic bubble memories offer an attractive trade-off in cost, storage density and access time. Being solid state they should have a greater long term reliability than the mechanically-driven discs and tapes they seek to replace. In addition, there is the exciting potential that logic functions can be performed on the bubble memory chip itself, thereby greatly increasing the flexibility and rate of handling data.

Of course, the first stage in such a technology is to find a class of materials which can support stable bubbles and allow their rapid manipulation. This article reviews the development of suitable single crystal materials and critically discusses how the properties of such materials are designed to obtain maximum performance from the magnetic bubble memory. We have not included the new class of amorphous materials which differ significantly from crystalline materials in both chemistry and structure but which nevertheless obey the same laws of bubble physics.

The opening section describes the bubble domain and presents the material requirements for the existence of stable bubble domains. Following sections trace the development of bubble-supporting materials and methods for the preparation of thin single crystal films of the most attractive of these materials, the garnet family. The static and dynamic behaviour of bubble domains and the engineering of garnet materials to give the optimum blend of these properties are then described in detail. Finally, a section is devoted to small ($\leqslant 1\ \mu$m in diameter) bubbles, which will be receiving more attention in the future.

2. Bubble domains

If a thin single crystal platelet of ferrimagnetic material has a unique easy axis of magnetization perpendicular to the plane of the platelet, then the material may exhibit magnetic domains bounded by 180° domain walls, as shown in Fig. 1a. These domains can be observed since they rotate the plane of polarized light in opposite directions, depending on their magnetic polarity, and so by correctly adjusting the analyser there is optical contrast between adjacent domains. The application of an external bias field parallel to the easy axis causes the domains whose net magnetization is aligned with the field to grow at the expense of those antiparallel to the field (Fig. 1b). On in-

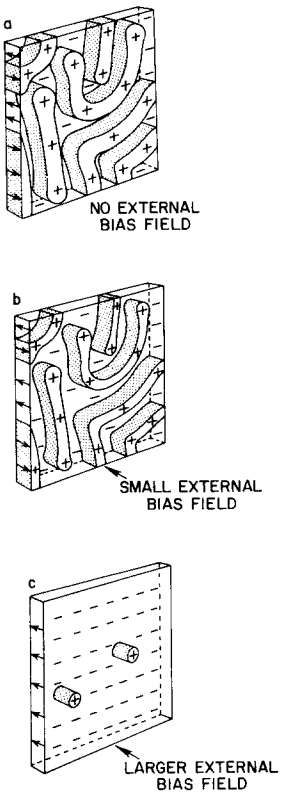

Figure 1 Generation of bubble domains [3].

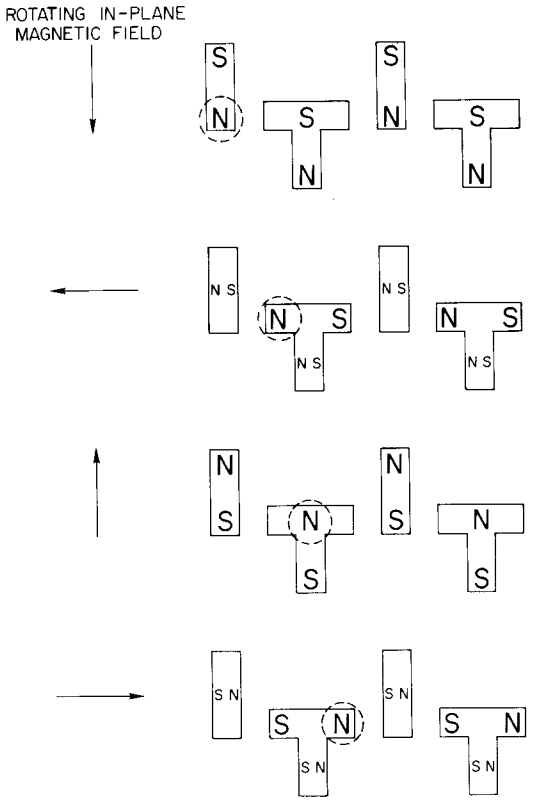

Figure 2 T and I bar bubble propagation track. The bubble has its magnetization pointing into the plane of the paper and consequently is attracted to the north pole of the permalloy T bar, deposited on the surface of the film. As the in-plane field is rotated, the direction of the permalloy magnetization follows that of the field and the bubble moves along the track in the sequence shown.

creasing the bias field some of the smaller domains contract ("run-in") to cylindrical (bubble) domains as in Fig. 1c. Raising the bias field still higher causes the bubbles to shrink and finally collapse when their diameter has shrunk to $\sim 1/3$ its original value. When all the bubbles have collapsed the platelet is completely magnetized in the direction of the bias field and is said to be saturated.

Since bubbles are stable over a moderate range of bias field conditions, circuits can be envisaged in which the presence or absence of a bubble defines the binary coding for data storage. In order to operate the simplest data storage circuit, the shift register, it is necessary that five basic functions can be performed with individual bubbles: nucleation; propagation; transfer between propagation tracks; detection; and annihilation. These basic functions are the subject of extensive literature (see, for example [3–8]). A T and I bar permalloy overlay circuit for propagation is shown in Fig. 2.

Clearly the density of data storage depends on the bubble diameter and the packing pattern in the device design. The latter influences access time along with data rate, which depends mainly on the spacing between bubbles and the velocity at which they can be moved. For an economical mass memory device, a minimum storage density of 10^5 bits cm^{-2} and a megabit data rate are desirable. Since the typical spacing of bubbles in a T–I bar device is four times the bubble diameter, 6 μm or smaller bubbles with domain wall velocities of at least a few hundred cm sec^{-1} per oersted drive field are required.

The theory of bubble domains has been developed by Thiele [9, 10] and may be summarized as follows:

(1) For the existence of stable *isolated* bubble domains, the material must have a unique easy axis of magnetization perpendicular to the plane of the platelet, such that the stability factor, q, is greater than unity, where

$$q = \frac{K_u}{2\pi M^2} \qquad (1)$$

K_u is the uniaxial perpendicular magnetic aniso-

tropy, and M is the magnetization. Alternatively this may be expressed in terms of the uniaxial anisotropy field, H_K

$$q = \frac{H_K}{4\pi M} \tag{2}$$

so that as long as the anisotropy field is greater than the saturation magnetization, $4\pi M$, the material may support stable bubbles.

(2) A bubble has its maximum stability when the film thickness (h) equals approximately $\frac{1}{2}$ of the bubble diameter (d) which leads to (3).

(3) The bubble diameter is given by

$$d \sim 8l = \frac{8(AK_u)^{\frac{1}{2}}}{\pi M^2} \tag{3}$$

where A is the exchange stiffness (a measure of the force acting to keep adjacent magnetic moments aligned) and l defines the characteristic length of the material. The quantity $4(AK_u)^{1/2}$ is the energy of the 180° domain wall.

(4) In order to move the bubble as an entity and with relative ease, the material must have a low coercivity, H_c, preferably less than 1% of its $4\pi M$.

In addition to satisfying Thiele's criteria, a bubble material must be capable of being manufactured into large area slices with reproducible magnetic properties and a high degree of crystalline perfection.

3. Materials search

3.1. Approach

Although it is obvious today that large area single crystal slices of a few microns thickness are most successfully prepared by epitaxial deposition onto a suitable substrate, the exploratory work to find suitable bubble materials was based on slices cut from bulk crystals grown mainly by the fluxed melt technique. This offered the most direct approach since it was not dependent on the development of epitaxial crystal growth techniques, neither was it limited by the lattice parameter nor the orientation of the substrate.

When discussing the development of bubble materials it is instructive to refer to Fig. 3, which was first published by Bobeck and Scovil [3] and shows the state of art at the time of its publication (June, 1971). The preferred material region is primarily defined by bubble diameters small enough to offer attractive storage densities yet not so small that their manipulation becomes a serious problem.

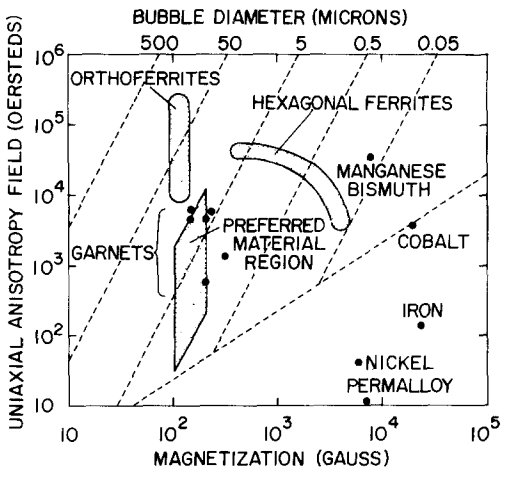

Figure 3 Analysis of Potential Bubble Materials [3]. The upper diagonal dashed lines denote constant bubble diameter. The lower diagonal dashed line is the limit where wall width = bubble diameter.

3.2. Orthoferrites

The first materials to receive interest were the rare earth orthoferrites. These are of general formula $RFeO_3$, where R is a rare earth or yttrium. They have a distorted perovskite structure making them essentially orthohombic. There are four crystallographically equivalent Fe^{3+} per unit cell.

The magnetic properties of this class of materials can be adequately described in terms of two magnetic Fe^{3+} sublattice strongly coupled antiferromagnetically and canted at a small angle, producing a net ferromagnetic moment perpendicular to the antiferromagnetic axis. Typically $4\pi M \sim 100$ G at 25° C. Since the room temperature H_K is much larger than $4\pi M$, they have a large q and support stable magnetic bubbles. There is extensive published literature on the magnetic properties of orthoferrites and their application to bubble mass memories [2, 11–16].

For optimum thickness slices, the bubble diameters of unsubstituted rare earth orthoferrites proved to be too large, typically 100 μm. Since bubble mobilities were of the desired magnitude, attempts were made to reduce the bubble diameter by increasing $4\pi M$ or reducing H_K. Since all of the Fe^{3+} are on crystallographically equivalent sites, increasing $4\pi M$ by selective substitution into only one of the Fe^{3+} magnetic sublattices appeared most unlikely. Robbins *et al.* [17] reported that the partial substitution of F^- for O^{2-} (0.2 to 0.3 atoms per formula unit) with charge compensation occurring by Ni^{2+} or Fe^{3+} sites, altered the antiferromagnetic canting angle so as to increase

$4\pi M$. However, the preparation of suitably sized crystals with uniform magnetic properties was never achieved.

A more successful method of obtaining smaller bubble diameters was by reducing H_K. Upon reducing the temperature of most rare earth orthoferrites, the anisotropy field first decreases in magnitude before passing through zero at the reorientation temperature where the magnetic easy direction changes from the $c\langle 0\,0\,1\rangle$ axis to the $a\langle 1\,0\,0\rangle$ axis. Further reduction in temperature results in an increased H_K along the a axis. For most unsubstituted orthoferrites, except $SmFeO_3$, the reorientation temperature is below room temperature. Therefore, by using Sm-substituted rare earth orthoferrites reorientation temperatures in the vicinity of room temperature were obtained. The reduction in H_K gave bubbles as small as 20 μm in these systems. (In Fig. 3 the uppermost dashed diagonal lines represent bubble diameter.) Bobeck *et al.* [12] operated shift registers with $Sm_{0.55}Tb_{0.45}FeO_3$, which supported $\sim 25\,\mu$m diameter bubbles. However, because of the proximity of the reorientation temperature with room temperature, the magnetic properties such as the bubble diameter and collapse field were strongly dependent on the device operating temperature. Since orthoferrites only support larger bubbles they have been largely replaced by garnets.

3.3. Hexagonal ferrites

The hexagonal ferrites based on the magnetoplumbite structure are mainly ferrimagnetic and usually contain more than two magnetic sublattices. Their complex layered hexagonal structure was established by Braun [18]. Generally, their magnetic easy axis is either the hexagonal axis itself or lies in the hexagonal basal plane. In 1960 Kooy and Enz [19] showed the existence of bubbles in magnetoplumbite platelets.

Magnetoplumbite ($PbFe_{12}O_{19}$) and its Ba and Sr analogs have a $4\pi M \sim 4000$ G and $H_K \sim 10^4$ G, the hexagonal axis being a unique easy axis of magnetization. Consequently, platelets parallel to the basal plane support stable magnetic bubbles, whose diameters are $< 1\,\mu$m and typically $\sim 0.2\,\mu$m. Although $4\pi M$ has been reduced by the partial substitution of Ga^{3+}, Al^{3+}, Cr^{3+} or Rh^{3+} for Fe^{3+} [20] to give bubble diameters as large as 10 μm, these materials all had extremely low bubble mobilities. Bobeck [21] reported initial domain wall mobilities of only ~ 1 to 10 cm sec^{-1} Oe^{-1} and limiting velocities in the range 100 to 600 cm sec^{-1}. It is not clear if these inferior dynamic properties are intrinsic or were the result of defects. The advent of garnets for bubble applications has overshadowed the hexagonal ferrites and no further work on their bubble mobility limitation has been reported.

3.4. Garnets

The rare earth iron garnets were first reported by Bertaut and Forrat [22] and, independently, by Geller and Gilleo [23]. Rare earth iron garnets are of formula $R_3Fe_5O_{12}$, and belong to the cubic crystal class (space group $Ia3d$). In each unit cell there are eight formula units with the 96 oxygen ions packed in such a way as to create 24 interstices which are 8-co-ordinated (dodecahedral), 16 which are 6-co-ordinated (octahedral) and 24 which are 4-co-ordinated (tetrahedral). The rare earth and yttrium ions occupy the larger dodecahedral sites and the Fe^{3+} occupy the smaller octahedral and tetrahedral sites. Consequently, the garnet unit may be written as $\{R_3\}[Fe_2](Fe_3)O_{12}$, where $\{\}$, $[\,]$ and $(\,)$ signify dodecahedral, octahedral and tetrahedral sites respectively. Because of their size, the larger rare earth ions (Pr^{3+}, Nd^{3+}) and also La^{3+} and Bi^{3+} can only partly substitute on dodecahedral sites.

The magnetic properties can be described by a three sublattice Néel model; $\{R_3\uparrow\downarrow\}[Fe_2\uparrow](Fe_3\downarrow)O_{12}$. The magnetic moments of the tetrahedral Fe^{3+} are all aligned and antiparallel to those of the octahedral Fe^{3+}. The alignment of the rare earth magnetic moments depends on the rare earths, being parallel to the tetrahedral Fe^{3+} for Nd^{3+} and Pr^{3+} and parallel to the octahedral Fe^{3+} for the ions Gd^{3+} through to Yb^{3+}. For diamagnetic R-ions (La^{3+}, Lu^{3+}, Y^{3+}) the net moment of the garnet is 5 Bohr-Magnetons at 0° K since each Fe^{3+} has five unpaired electrons.

Initially the ferrimagnetic garnets were not considered as magnetic bubble materials because garnets are intrinsically cubic with four equivalent $\langle 1\,1\,1\rangle$ magnetic easy axes. (A bubble material must be uniaxial.) However, during 1970 it was reported [24] that in garnet crystals containing two or more R-ions, the R-ions can show a non-random distribution on the six inequivalent types of dodecahedral sites. Thus the material is no longer perfectly cubic, but is uniaxial instead. One of the $\langle 1\,1\,1\rangle$ axes is then a unique easy axis and appropriately oriented slices of certain garnet com-

positions are capable of supporting stable bubble domains.

Since the garnet structure is stable over a wide lattice parameter range (~ 11.5 to ~ 13 Å) it can support a wide variety of substitutional atoms, allowing these materials to be designed for specific properties. When Ga^{3+} or Al^{3+} substitute for Fe^{3+}, they show ~ 90% preference for tetrahedral sites and therefore are efficient in reducing $4\pi M$. Anisotropy H_K depends on the combination of rare earths, the crystal growth conditions and the orientation of the slice. In addition, many of the garnets have relatively temperature insensitive magnetic properties at room temperature and have high domain wall velocities as well. Consequently, a great deal of effort has been directed to the application of garnets for bubble mass memory devices, and indeed, the garnets are probably the most widely studied bubble materials today. The remainder of this article concentrates on garnet materials.

4. Crystal growth

4.1. Substrates

For small diameter bubbles to be stable, very thin crystals are required, and for mechanical strength it is necessary to support these magnetic garnet crystals on non-magnetic substrates. Nearly all garnets for device or physical studies are made epitaxially in thin film form on rare earth gallium garnet substrates [25]. Because of its close lattice parameter match with $Y_3Fe_5O_{12}$ ($a_0 = 12.376$ Å), the material upon which most of the garnet bubble materials are based, $Gd_3Ga_5O_{12}$ ($a_0 = 12.383$ Å) is the most commonly available substrate material. $Sm_3Ga_5O_{12}$ ($a_0 = 12.437$ Å) and $Nd_3Ga_5O_{12}$ ($a_0 = 12.506$ Å) are also used for substrates, although to a far lesser extent.

Rare earth gallium garnets, unlike the corresponding iron garnets, are congruently melting and can, therefore, be grown from the pure melt by directional freezing. Fortunately, when the need for substrates arose, crystal growers already had several years experience in producing $Y_3Al_5O_{12}$ for both jewelry and laser applications. Although the lattice parameter of $Y_3Al_5O_{12}$ itself ($a_0 = 12.02$ Å) is small to be used as a bubble substrate, the crystal growth expertise for $Y_3Al_5O_{12}$ is directly applicable to $Gd_3Ga_5O_{12}$.

$Gd_3Ga_5O_{12}$ melts at $> 1700^\circ$ C and is grown from rf heated iridium crucibles under an atmosphere of nitrogen and a few per cent oxygen. Single crystal boules are pulled from the melt by the Czochralski technique. Provided the correct growth procedures (see [26–30] for fuller details) are adhered to, up to 2 in. diameter, dislocation-free boules with extremely low levels of residual strain can be grown routinely. The boules are then cut into oriented slices which are lapped smooth with diamond or alumina abrasive and finally given a chemical-mechanical polish with Syton*, or some other alkaline colloidal polishing medium. Highly perfect substrates with a good degree of surface free of damage are essential since any defects will be replicated in the bubble film during its epitaxial deposition and will impair the motion of bubbles.

4.2. Film growth

Single crystal garnet films have been grown by chemical vapour deposition (CVD), hydrothermal epitaxy (HE), and liquid phase epitaxy (LPE).

Originally CVD was a strong contender for the garnet film growth process both because of the apparent ease with which it could be adapted for large scale film production and because the films produced were free from solvent contamination, which is not the case of LPE. The various stages in the CVD process are shown schematically in Fig. 4. Essentially it involves the vaporization of the rare earth, iron and gallium chlorides, which may have been prepared in situ, their transportation with an Ar or He carrier gas into the growth chamber where at temperatures ~ 1200° C they are reacted with oxygen to deposit garnet epitaxially on the sub-

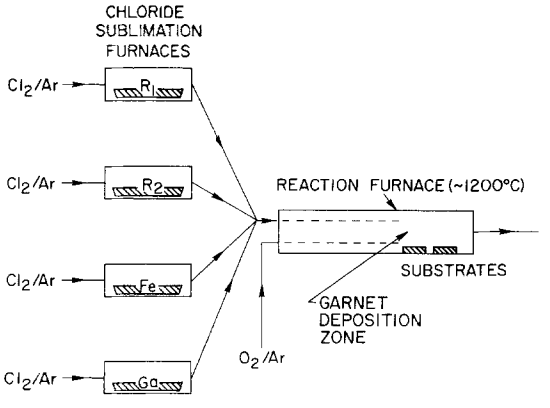

Figure 4 Chemical vapour deposition process (schematic).

* Syton is a registered trademark of the Monsanto Co, St. Louis, Mo.

strates according to the reaction

$$3RCl_{3(g)} + (5-x)\,FeCl_{2(g)} + x\,GaCl_{3(g)} + 6O_{2(g)} \xrightarrow{Ar} R_3Fe_{5-x}Ga_xO_{12} + \tfrac{1}{2}(19-x)\,Cl_{2(g)}. \quad (4)$$

A more complete description of the CVD process is given by Mee *et al.* [31], Stein [32], Robinson [33], Wilkins [34] and Taylor and Sadogopan [35].

Recently, interest in the CVD process has declined because the high growth temperatures required produce films with little or no growth-induced uniaxial anisotropy, limiting the process only to systems with substantial stress-induced anisotropy (see Section 5.1). Presumably high growth temperatures and long growth times mitigate against growth-induced anisotropy which can be annealed out by diffusion processes. In addition, defect densities are significantly higher in CVD films than in comparable films grown by LPE. Cowher *et al.* [36] have shown that the use of organometallics as transporting agents allows lower growth temperatures which may help lower defect densities and allow growth-induced anisotropy. However, much work remains to be done before CVD can reemerge as a contender to LPE.

Hydrothermal epitaxy has been used by Kolb and Laudise [37] and Ferrand *et al.* [38, 39]. The rare earth, iron and gallium oxides are dissolved in concentrated (20 M) NaOH at 500 atm and ~ 500° C. Garnet is deposited on substrates at the cooler end (~ 450° C) of the autoclave (Fig. 5). With certain modifications of the growth procedure, attack on the substrate prior to growth by the alkali can be minimized. Although HE has produced highly perfect films of the pure iron garnets, notably $Y_3Fe_5O_{12}$, uniform gallium substitution is a problem because of the high solubility of Ga_2O_3. In addition, the slow growth rates (~ 0.1 μm h^{-1}) are a limitation for the growth of most bubble films used today.

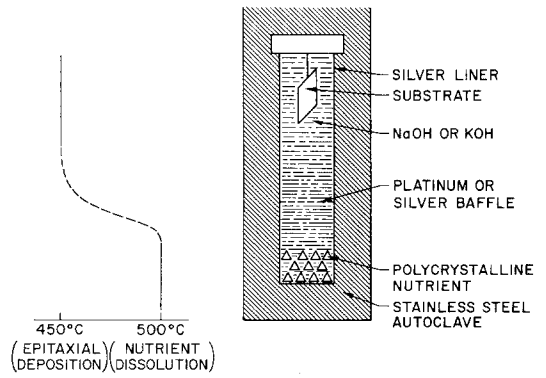

Figure 5 Hydrothermal apparatus for growth of garnet films [39]. Left hand side of diagram shows temperature at corresponding position in autoclave.

At the present time, LPE is the most successful growth process since it is suitable for a wide range of garnet compositions and can routinely produce films with extremely low or even zero defect densities. Film growth occurs by immersing the substrate into a supersaturated solution of granet by either dipping [40–42] or, less commonly, a tipping method [25, 43] as shown in Fig. 6. Generally the solvent is PbO–B_2O_3, although the BaO–BaF_2–B_2O_3 system has also been used [44–46]. Growth takes place isothermally and typically at a rate ~ 1 μm min^{-1}. Blank and Nielsen [47] have shown that smooth continuous films can be grown when the unstrained room temperature lattice parameter of the film is between 0.013 Å smaller and 0.018 Å larger than that of the substrate. Fortunately, mixed garnets obey Vegard's rule so that their lattice parameters can be interpolated from those of the pure garnet constituents. Small amounts of Pb^{2+} from the flux are incorporated on dodecahedral sites in the garnet

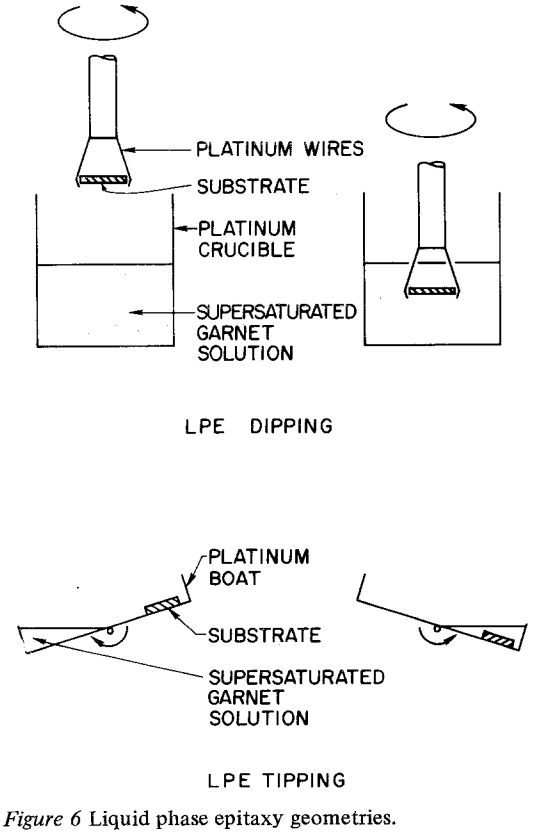

Figure 6 Liquid phase epitaxy geometries.

lattice, increasing the lattice parameter. However, this can be allowed for since the characteristics of Pb^{2+} incorporation have been well studied [48–50].

For further details of the LPE process the reader is referred to a recent review by Giess and Ghez [50].

5. Design of garnet bubble compositions

5.1. Magnetization and uniaxial anisotropy

Although it is realized that the ultimate aim of bubble technology is to produce devices utilizing submicron diameter bubble domains, so far most of the development has been with ~ 5 μm diameter bubbles. These are small enough to be economically attractive yet large enough to be seen in an optical microscope and to be manipulated using permalloy overlap patterns generated by conventional photolithographic techniques.

Ideally, bubble materials should satisfy Thiele's criteria (see Section 2) of $d \sim h/2$, where

$$d \sim 8l = \frac{8(AK_u)^{1/2}}{\pi M^2} \quad \text{and} \quad q = \frac{K_u}{2\pi M^2} \geqslant 1.$$

Therefore, for a given bubble diameter, the film thickness is specified. The exchange constant, A, essentially depends on the film Fe^{3+} content and for garnet systems of interest has values in the narrow range 1×10^{-7} to 4×10^{-7} erg cm^{-1} at room temperature. Consequently, the main design variables are $4\pi M$ and K_u and even these are subject to restrictions since for a given device design there is an optimum value for q. For T–I bar propagation mechanisms, a $q \geqslant 5$ is necessary to prevent spurious bubble nucleation at high drive fields. A 5 μm bubble in a system with $q \sim 5$ requires $4\pi M \sim 130$ to 200 G and $K_u \sim 3000$ to 8000 erg cm^{-3}. For some gapless propagation structures such as the contiguous disc [51, 52] or the bubble lattice file [53] a lower q value may be acceptable; although this has yet to be demonstrated.

The properties of the pure rare earth iron garnets are given in Table I. (The values for the hypothetical garnet $La_3Fe_5O_{12}$ were estimated.) For mixed garnet systems these properties are approximately additive. Generally, to reduce $4\pi M$ to the deisred range of 130 to 200 G, ~ 1 Fe^{3+} per formula unit must be substituted by Ga^{3+}. Fig. 7 illustrates how

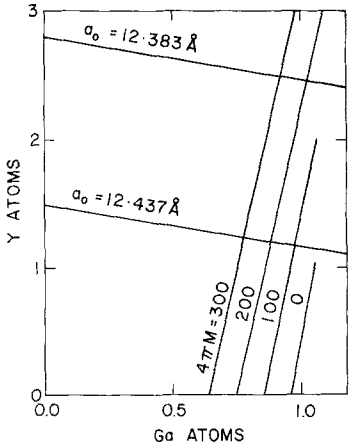

Figure 7 Magnetization and lattice mismatch in the $(Eu, Y)_3(Fe, Ga)_5O_{12}$ system [63].

TABLE I Iron garnet physical constants

	λ_{111} (× 10^{-6})	λ_{100} (× 10^{-6})	K_1 (× 10^3)	$4\pi M$ (G)	T_x (K)	T_c (K)	a_0 (Å)	λ' (× 10^{-7})
La	− 2.4	− 1.4			none		12.767	0.52
Sm	− 8.5	+21.0	−20	1675	none	578	12.529	12
Eu	+ 1.8	+21.0	−37	1172	none	566	12.498	2.1
Gd	− 3.1	0.0	− 6	56	286	564	12.471	0.52
Tb	+12.0	− 3.3	− 6	198	248	568	12.436	48
Dy	− 5.9	−12.6	− 6	376	225	563	12.405	26
Ho	− 4.0	− 3.4	− 6	882	140	567	12.375	42
Y	− 2.4	− 1.4	− 5.7	1767	none	553	12.376	0.52
Er	− 4.9	+ 2.0	− 6	1241	83	556	12.347	7
Tm	− 5.2	+ 1.4	−11	1397	none	549	12.323	1.2
Yb	− 4.5	+ 1.4	− 7	1555	5	548	12.302	4.2
Lu	− 2.4	− 1.4	− 5.2	1815	none	549	12.283	0.52

Magnetostriction coefficients (λ_{111} and λ_{100}) are from [55] and [56].
Cubic anistropy constants (K_1 in erg cm^{-3}) are from [57] and [58].
$4\pi M$ are from [58].
Compensation temperatures (T_x) are from [59].
Curie temperatures (T_c) are from [60].
Lattice parameters (a_0) are from [61].
Rare earth damping parameters (λ' in Oe^2 sec rad^{-1}) are from [62].

in the $Eu_xY_{3-x}Fe_{5-y}Ga_yO_{12}$ system both the $4\pi M$ and the lattice parameter requirements can be simultaneously satisfied (the lattice parameters 12.383 and 12.437 Å correspond to $Gd_3Ga_5O_{12}$ and $Sm_3Ga_5O_{12}$ substrates respectively).

In garnet films the uniaxial anisotropy, K_u, may be derived from two mechanisms; growth-induced and stress-induced anisotropy. Stress-induced anisotropy arises when the unstrained lattice parameters of the film and substrate are not perfectly matched. Because of the large garnet lattice parameter, and consequently the large Burger's vector, it is difficult to generate dislocations at the film/substrate interface which, therefore, remains perfectly coherent; i.e. when viewed along the perpendicular direction, film atoms are in register with the substrate atoms. To accommodate the mismatch the film relaxes in the direction perpendicular to the interface [31], distorting its cubic structure. The stress-induced anisotropy, K_S, is given by;

$$K_S = -\tfrac{3}{2}\sigma\lambda \tag{5}$$

where σ is the biaxial (planar) stress in the film and λ is the magnetostrictive coefficient. Values of λ for the (1 1 1) and (1 0 0) garnet planes are given in Table I. The biaxial stress in the film can be written in terms of its elastic constants and the lattice mismatch with the substrate

$$\sigma = \frac{E}{1-\nu}\frac{\Delta a}{a_0} \tag{6}$$

where E is Young's modulus ($\sim 2 \times 10^{12}$ dyn cm^{-2}) and ν is Poisson's ratio (~ 0.29). Consequently, K_S is approximately given by Klokholm's expression [54]

$$K_S \approx \frac{-10^{12}\lambda\Delta a}{2.9} \tag{7}$$

so that for positive values of Δa (i.e. film in biaxial tension) the film must have a net negative λ to exhibit a positive (uniaxial) K_S.

Growth-induced anisotropy (K_g) is more complex to treat quantitatively. As previously suggested, rare earth ordering appears to play a major role [64]. However, other mechanisms have been suggested [65–68] and the experimental evidence indicates that more than one of these mechanisms may be responsible. Qualitatively, rare earth ions which have a net orbital angular momentum (especially Sm^{3+}, Eu^{3+}, Pr^{3+}, Nd^{3+} and Tb^{3+}) provide a large contribution to K_g whereas those with no net orbital angular momentum (Gd^{3+}, Lu^{3+}, Y^{3+}, La^{3+}) have a lesser effect. In addition, there is a tendency for K_g to increase as the difference in ionic radii of the rare earths increases [24].

The total uniaxial anisotropy is given by the sum of the K_S and K_g components which, depending on the system, may act with or in opposition to each other. Giess and Cronemeyer [69] have experimentally verified this using the same film composition grown onto a series of substrates with a wide range of lattice parameters. Without growth induced anisotropy the range of useful garnet compositions would be severely limited. Also it should be noted that cubic (magnetocrystalline) anisotropy, K_1, can contribute to the effective K_u.

For bubble materials with $4\pi M \sim 130$ to ~ 200 G, the required magnitude of K_u can be generated by many combinations of rare earths using appropriate growth conditions and lattice mismatch. Since those R-ions which have no net orbital angular momentum provide very little resistance to domain wall motion, most 5 μm bubble compositions are based on these. Compositions of the type $R_xY_{3-x}Fe_{5-y}Ga_yO_{12}$ ($0.9 \leqslant y \leqslant 1.2$) are of particular interest where R = Eu [41], Sm [42, 70] or La [42] since lattice matching with $Gd_3Ga_5O_{12}$ can be achieved with $x \leqslant 0.6$. Compositions involving three R-ions are also popular, allowing an extra degree of freedom in materials design at the expense of a more complex growth system. Gd–Y–Yb [71, 72], Eu–Y–Yb [73] and Eu–Y–Tm [74] are examples of such systems.

5.2. Temperature dependence of magnetic properties

In a bubble device the operating margins will be significantly reduced if the magnetic properties of the material, in particular the bubble diameter and collapse field, are sensitive to temperature fluctuations. Both the bubble diameter and collapse field depend on $4\pi M$, A and K_u, all of which are complex functions of temperature and in turn depend on the garnet composition. Therefore, the approach to temperature insensitive properties is semi-empirical and is based on the material not having a magnetic transition temperature in the vicinity of room temperature.

Table I gives the Curie temperatures, T_c, of unsubstituted rare earth iron garnets. Typically these are $\sim 280°$ C. However, T_c depends on the garnet Fe^{3+} content so that when ~ 1 Ga^{3+} atom is substituted to reduce the $4\pi M$, T_c is lowered to $\sim 140°$ C. Ga^{3+} substitution is not the ideal method

for reducing $4\pi M$ since only $\sim 90\%$ resides on tetrahedral sites. The remaining $\sim 10\%$ resides on octahedral sites thereby partly counteracting the tetrahedral Fe^{3+} dilution. Bonner *et al.* [74] have grown films containing Si^{4+} and Ge^{4+}. These reside $\sim 99\%$ on tetrahedral sites and are, therefore, almost 20% more efficient in reducing $4\pi M$. Charge compensation occurs by Ca^{2+} or Sr^{2+} occupying dodecahedral sites. Bonner's films have $T_c \sim 190^\circ$ C and consequently the temperature dependence of their magnetic properties is relatively small. A further consequence of the greater Fe^{3+} content in the Si^{4+}/Ge^{4+} substituted films is their higher exchange constant which increases both the bubble mobility and its critical velocity (see Section 5.3). The advantages of Si^{4+}/Ge^{4+} substitution are partly offset since films are more complex to grow reproducibly than their Ga^{3+} containing counterparts [70, 75]. The control of growth temperature is especially critical.

In addition to a Curie temperature, some garnets also exhibit a compensation temperature (T_x in Table I). This occurs when the rare earth has a sufficiently large magnetic moment aligned with the octahedral Fe^{3+} sublattice so that the resultant moment is greater than that of the tetrahedral Fe^{3+} sublattice at 0° K. Since the magnetic moments of certain rare earths decrease more rapidly with temperature than the Fe^{3+} moment, there is a temperature (T_x) at which the opposing sublattice moments are exactly equal and $4\pi M = 0$. Garnets with T_x in the vicinity of room temperature, such as $Dy_3Fe_5O_{12}$, $Tb_3Fe_5O_{12}$ and, in particular, $Gd_3Fe_5O_{12}$ have magnetic properties strongly dependent on the temperature, but they can sometimes be used to advantage in bubble film compositions because they give lower $4\pi M$. This reduces the level of Ga^{3+} substitution needed, resulting in higher Curie temperatures and exchange constants.

5.3. Bubble velocity

In a working bubble memory the rate at which the data can be accessed depends on both the device design and the speed at which the bubbles can be moved. The velocity, V, of a bubble is given by [9]

$$V = \frac{\mu}{2}\left(\Delta H - \frac{8}{\pi} H_c\right) \qquad (8)$$

where μ is the domain wall mobility ($cm\,sec^{-1}\,Oe^{-1}$), ΔH is the field gradient across the bubble and H_c is the coercivity of the garnet film. The requirement that H_c be less than 1% of $4\pi M$ is met by most good quality garnet films. Since it is desirable to move the bubble rapidly using the lowest possible drive field, the coercivity should be low and the mobility high.

As yet there is no quantitative model for coercivity and values vary according to the measurement technique. For a given garnet composition it seems that low coercivity is associated with high crystalline perfection and magnetic uniformity. Also coercivity appears to scale with anisotropy. The factors which determine the relative coercivity for different garnet compositions are not fully understood.

Mobility, on the other hand, is better understood. Vella-Coleiro *et al.* [62] have determined the relative magnitudes of the rare earth damping parameters, λ', for most unsubstituted rare earth iron garnets, both by bubble dynamics and by ferrimagnetic resonance (the damping parameter is approximately proportional to the ferrimagnetic linewidth). Mobilities are inversely proportional to the damping parameters, values of which are given in Table I. As a rough guide, when the ions occupying dodecahedral sites have no net orbital angular momentum (Gd^{3+}, Lu^{3+}, Y^{3+}, La^{3+}, Ca^{2+}) the resistance to domain wall motion is least. Using these ions, mobilities approaching $2000\,cm\,sec^{-1}\,Oe^{-1}$ have been achieved [70].

When moving bubbles at high speeds there is, however, a severe limitation. Bubble velocity increases with increasing drive field until a critical velocity, V_c, is reached. Attempting to move the bubble faster than V_c by the use of higher drive fields causes erratic bubble propagation. The phenomenon has been explained in terms of the domain wall structure by Slonczewski [76] and Hagedorn [77]. Since the domain wall separates two domains which are magnetized in opposite directions, the magnetization must rotate by 180° through the thickness of the domain wall. In Fig. 8, if the magnetization rotates about the x-axis, we have a pure Néel wall and if it rotates about the y-axis we have a pure Bloch wall. Because the bubble domain wall width is much less than the film thickness, a Bloch wall is energetically more favourable. However, the stray magnetic fields from the poles at the surface of domains induce Néel character at the surfaces of the domain walls. As the domain wall is moved faster the structure becomes less stable and eventually at the critical

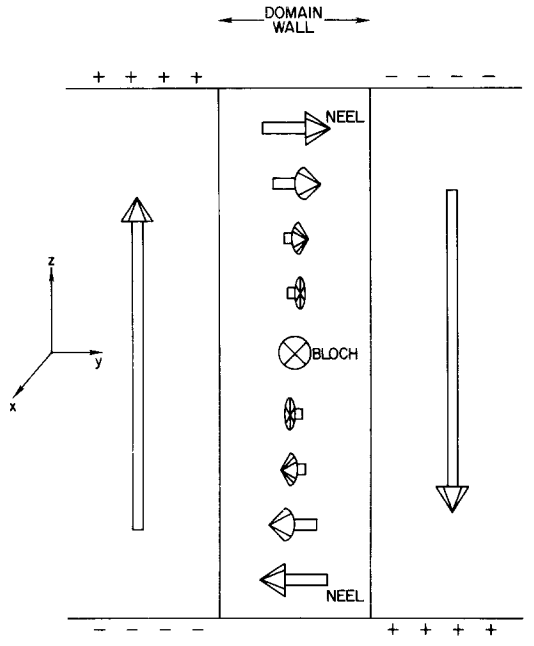

Figure 8 Section through a bubble domain wall [76].

velocity, horizontal Bloch lines* are generated at the film surface. These can then move through the domain wall and annihilate at the opposite surface. The generation and passage of the horizontal Bloch lines through the domain wall causes the erratic bubble propagation.

The critical velocity for a planar domain wall is given by

$$V_c = \frac{24\gamma A}{hK_u^{1/2}} \qquad (9)$$

where γ is the gyromagnetic ratio ($=ge/(2mc)$, where g is the spectroscopic splitting factor, e is the absolute value of the electronic charge, m is the mass of the electron and c is the velocity of light). For almost all 5 μm bubble materials $g \sim 2$. K_u, A and h are only slightly variable since they determine bubble diameter and stability. Therefore, V_c is generally $\sim 2000\,\mathrm{cm\,sec^{-1}}$.

For the $Eu_3Fe_{5-x}Ga_xO_{12}$ system, LeCraw *et al.* [78] have shown that the effective g factor is given by

$$g = M_{Eu} + M_{Fe}/(M_{Eu}/g_{Eu} + M_{Fe}/g_{Fe}) \qquad (10)$$

where M_{Eu} and g_{Eu} are the magnetization and g factor of the Eu^{3+} sublattice and M_{Fe} and g_{Fe} are the *net* magnetization and g factor for the combined octahedral/tetrahedral Fe^{3+} sublattices. Eu^{3+} has a $J = 0$ ground state but also has a moment induced by the exchange field in the garnet lattice. Since M is proportional to the product of g and J, therefore $g_{Eu} \gg 2$ as shown by LeCraw and Blank [79]. For the case where $x = 0$, $M_{Fe} \sim M_{YIG} \sim 1700$ G and $M_{Eu} \sim (M_{YIG} - M_{EuIG}) \sim 500$ G, where M_{YIG} and M_{EuIG} are the magnetizations of $Y_3Fe_5O_{12}$ and $Eu_3Fe_5O_{12}$ respectively, and consequently $g \sim g_{Fe} \sim 2$. An interesting situation occurs when $x \sim 1.2$. In this case, 1.1 Ga^{3+} reside on the tetrahedral Fe^{3+} sublattice, 0.1 Ga^{3+} reside on the octahedral Fe^{3+} sublattice and so $M_{Fe} \sim 0$ and $g \sim g_{Eu}$ from Equation 10. The composition thus has a high gyromagnetic ratio and a correspondingly large critical velocity. It should be noted, however, that the initial bubble mobility is independent of the gyromagnetic ratio (see Equation 12).

LeCraw *et al.* [79] have very recently extended this approach using Ge^{4+}/Si^{4+} rather than Ga^{3+} substitution because of the higher T_c realized with the former. Their exact composition was $Eu_{1.45}Y_{0.45}Ca_{1.1}Fe_{3.9}Si_{0.6}Ge_{0.5}O_{12}$. Although this appears to be a complex system, it is instructive to analyse the reasons for their choice; the 1.1 ($Si^{4+} + Ge^{4+}$) ions are needed for $M_{Fe} = 0$ and an equivalent amount of Ca^{2+} is needed to charge compensate the tetravalent ions. The 1.45 Eu^{3+} ions give the material a $4\pi M \sim 200$ G. The remaining dodecahedral sites are filled with Y^{3+} since it both enhances bubble mobility and does not contribute to the $4\pi M$. The Si^{4+}/Ge^{4+} ratio is chosen so that the film has a good lattice parameter match with the $Gd_3Ga_5O_{12}$ substrates.

For LPE grown films of this composition, LeCraw and Blank [79] report g factors in excess of 30. Corresponding critical velocities are as high as $30\,000\,\mathrm{cm\,sec^{-1}}$, an order of magnitude greater than for other 5 μm bubble compositions. It therefore appears as if this type of garnet composition is very attractive for high speed devices. LeCraw and Blank point out that the g factor itself is not strongly temperature dependent and the T_c ($\sim 190°$ C) is high enough to expect good temperature stability of the bubble diameter and collapse field.

5.4. Hard bubbles

One of the major problems in magnetic bubble technology has been the existence of "hard bubbles". Hard bubbles are those which contain a large number of vertical Bloch lines in their wall

* A Bloch line marks the transition between Bloch and Néel segments in the bubble domain wall. In Fig. 8, there is one pair of Bloch lines.

structure [80, 81]. Certain behavioural characteristics distinguish these from normal bubbles, which contain no vertical Bloch lines. In a drive field gradient, hard bubbles propagate at an angle to the direction of the drive field. The larger the number of vertical Bloch lines, the greater is the deflection angle and consequently the lower is the effective bubble mobility in the direction of the drive field. Furthermore, hard bubbles collapse at a higher value of bias field than do normal bubbles. Although in the recently-proposed bubble lattice file mode of data storage, these Bloch lines may be utilized for the binary coding [82], generally the presence of hard bubbles is detrimental to device operation.

Hard bubble suppression can be achieved by the use of a double layer film structure [83]. Adjacent to the upper or lower surface of the bubble film there is a thin (~ 20% of the film thickness) capping layer whose magnetic properties differ from those of the bubble film. The two alternative forms of the capping layer, the 90° and 180° caps, are shown in Fig. 9. In both cases the planar domain wall at the interface of the bubble film and capping layer prevents the formation of a large number of Bloch lines in the bubble domain wall.

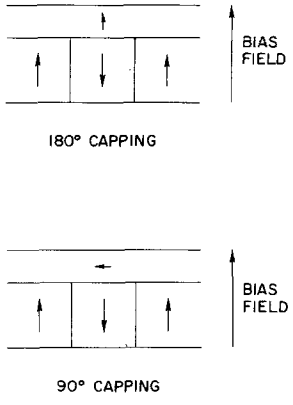

Figure 9 90° and 180° capping layers for hard bubble suppression.

The 180° capping layer is simply comprised of a garnet material whose $4\pi M$ is lower than that of the bubble film. At the bias fields required for the existence of bubbles, the capping layer is completely magnetized in the direction of the bias field thus forming a 180° planar domain wall at the interface with the bubble film. The 90° capping layer can either be fabricated using a garnet composition which has in-plane anisotropy (i.e. $K_u < 0$) or by ion-implantation to a shallow depth in the bubble film. Hard bubble suppression by hydrogen ion implantation is described by Wolfe *et al.* [84, 85]. The implantation merely causes an expansion of the garnet lattice. Thus if the film is in planar tension, sufficient implantation can cause the surface layer to be in planar compression. For garnet materials with a large negative magnetostrictive coefficient, K_u of the surface layer may become negative and its magnetization then lies parallel to the plane of the film. As in semiconductor technology, the incident energy of the implanted species determines the penetration depth and the dosage determines the degree of lattice expansion. The use of larger implanted species (e.g. neon ions) has the advantage of requiring a lower dosage, thus reducing the processing time.

5.5. Smaller bubbles

Because magnetic bubbles are a solid state technology, 5 μm diameter bubbles have potential for data storage, especially in systems where long term reliability is a prime requirement (e.g. telephone switching, space flight recorders). In the computer industry there are different trade-offs to consider. For optimum performance, large scale computers utilize a combination of memory units, each with different cost/access time/storage density characteristics. In such a system, magnetic bubbles offer faster access time than the conventional discs and tapes they seek to replace. On the other hand, discs and tapes can have storage capacities which can only be matched with small ($\leqslant 1\,\mu$m diameter) bubbles. Since the typical bubble spacing in a device is approximately four times the bubble diameter, smaller bubbles have the further advantage of having less distance to move than their larger counterparts to achieve comparable data rates and access times.

Recent advances in both electron beam [86] and X-ray lithography [87] have made possible the reliable fabrication of overlay circuits for the manipulation of ~ 1 μm diameter bubbles. In the near future it seems possible that a technology with even smaller (~ 0.5 μm) bubbles can be realized. Of course, to achieve such small bubbles poses a number of materials problems, quite distinct from those associated with ~ 5 μm bubbles, e.g. thinner films require special growth considerations [50]. This section critically discusses these problems, outlines the present state of the art and speculates on possible future developments.

As was the case with 5 μm bubble materials, Thiele's criteria are the ground rules for designing

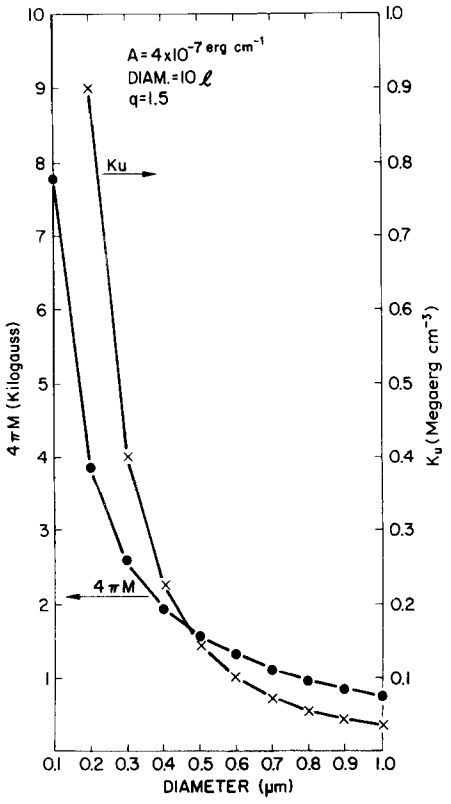

Figure 10 Magnetization and uniaxial anisotropy for submicron bubbles. Projected from data for $EuYb_2Fe_5O_{12}$.

smaller bubble materials. To obtain smaller bubbles the garnet must have a larger $4\pi M$. This in turn requires larger values of K_u to satisfy the condition $q \geqslant 1$. To put this into the correct perspective it is necessary to consider Fig. 10. Here, a bubble diameter of 10 times the characteristic length, an exchange constant of 4×10^{-7} erg cm^{-1} and a q of 1.5 (which is probably the minimum q value that any practical device can operate with) are assumed. Clearly the smallest bubble diameter that can be achieved for garnets is limited by $4\pi M$. Rare earth iron garnets have a maximum $4\pi M \sim 1800$ G (Table I). Although substitution in the octahedral Fe^{3+} sublattice (e.g. by Sc^{3+}) can be used to further increase $4\pi M$, spin canting occurs even at moderate levels of substitution, limiting the $4\pi M$ to ~ 2000 G and consequently the bubble diameter to $\sim 0.4\,\mu$m.

More significant is that as the bubble diameter decreases, the K_u required to maintain a given q increases rapidly, as the square of $4\pi M$. Fortunately, K_u itself is not an absolute constant. For the $Eu_1Tm_2Fe_{5-x}Ga_xO_{12}$ system, Giess *et al.* [88] grew a series of films using almost identical growth conditions varying only Ga concentration $0 \leqslant x \leqslant 1.2$. It was found that although K_u does increase slightly with $4\pi M$, this alone is not sufficient to maintain high q values when the submicron region is approached as $x \to 0$.

From Equation 7 it is clear that for most practical bubble materials, even with the most favourable lattice mismatch conditions, $K_S \sim 10^4$ erg cm^{-3}. Consequently, the majority of K_u required for $\leqslant 1\,\mu$m diameter bubbles must be derived from a growth-induced mechanism. Experience with $5\,\mu$m bubble garnets has shown that Eu^{3+} and Sm^{3+} are particularly efficient in increasing K_g. Bearing in mind that a large difference in the ionic radii of the rare earths in the film promote a large K_g, Giess *et al.* [89] investigated film compositions where either Sm^{3+} or Eu^{3+} was paired with Yb^{3+} or Lu^{3+}. The Yb^{3+} substituted films (e.g. $EuYb_2Fe_5O_{12}$) have $4\pi M \sim 1400$ G, $K_u \sim 10^5$ erg cm^{-3} and support $0.5\,\mu$m bubbles with a $q \sim 2$. The Lu^{3+} substituted films also support $0.5\,\mu$m bubbles, albeit with a slightly lower q. When $4\pi M$ is reduced to ~ 700 G by partial Ga^{3+} substitution, these films support $1\,\mu$m bubbles with $q \sim 4$. Very recent work has shown that Tm^{3+} can be used instead of Yb^{3+} in these film combinations with virtually no loss in q yet quite a substantial gain in bubble mobility.

Plaskett *et al.* [68, 90] have grown films of composition $Eu_2Y_1Fe_5O_{12}$ and $Eu_3Fe_5O_{12}$ onto $Sm_3Ga_5O_{12}$ and $Nd_3Ga_5O_{12}$ substrates respectively. At low growth temperatures ($\sim 750^\circ$ C) these films contain almost 6% by weight of Pb^{2+} from the flux. The presence of Pb^{2+} increases K_u in these films, the effect being far greater for films of (1 0 0) orientation than those of (1 1 1) orientation. For Eu^{3+}, λ_{100} is an order of magnitude greater than λ_{111}. However this only partially explains the large K_u of the (1 0 0) oriented films. In fact, these films exhibit the highest values of K_u ($\sim 2 \times 10^5$ erg cm^{-3}) yet reported for garnets and support $0.5\,\mu$m bubbles with a q of 3. However, even this q value may not be sufficient for some device applications and at present work is in progress to increase the q in submicron bubble garnet compositions.

These $0.5\,\mu$m bubble compositions contain no Ga^{3+} and have $T_c \sim 280^\circ$ C while $1\,\mu$m bubble compositions contain ~ 0.5 Ga^{3+} per formula unit and have $T_c \sim 220^\circ$ C. Because of these high values of T_c both the bubble diameter and collapse field are less sensitive to the operating temperature than is the case for $5\,\mu$m bubble materials. Typically, for submicron bubble garnets both the

bubble diameter and collapse field decrease by $\sim 0.2\%$ for each 1° C increase in the operating temperature.

As previously stated, for a given bubble velocity the data rate increases and access time decreases with decreasing bubble diameter. Bubble mobility is given by [62]

$$\mu = \frac{\gamma}{\alpha}\left(\frac{A}{K_u}\right)^{1/2} \qquad (11)$$

where α is the Gilbert damping parameter ($= \gamma\lambda'/M$) and λ' is the Landau–Lifshitz damping parameter $\div \gamma^2$. Therefore, Equation 11 can be rewritten as

$$\mu = \frac{M}{\lambda'}\left(\frac{A}{K_u}\right)^{1/2} = \frac{1}{\lambda'}\left(\frac{A}{2\pi Q}\right)^{1/2}. \qquad (12)$$

Although going to smaller bubbles increases A, the rare earths required to generate sufficient K_u have high values of λ'. Hu and Giess [91] measured a mobility of 800 cm sec^{-1} Oe^{-1} for the $Eu_1Tm_2Fe_{4.5}Ga_{0.5}O_{12}$ system. The Sm^{3+} analog has a somewhat lower mobility.

As with 5 μm bubbles it is the critical velocity rather than bubble mobility that limits high speed operation. From Equation 9, $V_c \sim 2000$ cm sec^{-1}. The approach of LeCraw *et al.* [79], to raise V_c by increasing γ, is limited by the $4\pi M$ that can be achieved using only the Eu^{3+} sublattice. The Si^{4+}/Ge^{4+} substituted films can contain a maximum of 1.9 Eu^{3+} which probably limits the $4\pi M$ to < 300 G and the bubble diameter to a minimum of ~ 3 μm. It is interesting to speculate here on the design of a related garnet. Replacing Si^{4+}/Ge^{4+} by Ga^{3+}/Al^{3+} would eliminate the need for charge compensation with Ca^{2+}. The resulting $Eu_3Fe_{3.8}(Ga, Al)_{1.2}O_{12}$ system might have $4\pi M$ as high as 500 G, a bubble diameter as small as 2 μm and could be grown on to $Nd_3Ga_5O_{12}$ substrates. Sufficient K_u presumably could be induced by the incorporation of Pb^{2+} from the flux. However, since the T_c for this system will be relatively low ($\sim 120°$ C), the bubble diameter and collapse field will be more sensitive to temperature fluctuations than comparable Si^{4+}/Ge^{4+} compositions.

Finally, we must consider hard bubbles and their suppression in submicron bubble films. Because this topic is still in its infancy, this section will be limited to a few general comments. Both the translational and the static collapse behaviour characteristic of hard bubbles are observed in submicron bubble films. Since the garnet compositions supporting stable submicron bubbles have a large K_u it is as yet uncertain whether ion-implantation can be used for hard bubble suppression. One would certainly expect the dosage required to create the in-plane magnetization of the surface layer to be higher than for ~ 5 μm bubbles. Whether this dosage can be achieved without damaging the film remains to be proven. The double layer film structure involving either a 90° or 180° capping layer may be the more effective approach to hard bubble suppression.

6. Conclusions

During the past seven or eight years, magnetic bubble technology has progressed from a mere concept to working hardware and engineering prototypes. The low cost, high performance and apparent reliability of the bubble memory make it an attractive solid state alternative to mechanically-driven discs and tapes. One of the major reasons for this remarkable progress has been the rapid development of suitable bubble materials which can be controllably fabricated into large area, single crystal films with a high degree of physical perfection. The methods of fabricating thin films from the most suitable class of these materials, the garnet family, are present and the engineering of garnet materials to obtain the desired physical properties is quite well understood. Emphasis is being placed upon the static and dynamic behaviour of bubble domains and the trade-offs that must be made to achieve the optimum device performance.

As well as the benefits to magnetic bubble technology itself, much of the basic research performed in developing this technology has greatly enhanced our understanding of materials preparation, properties and device fabrication in general. In crystal growth, for example, detailed investigations of the LPE process have enabled the film growth mechanism to be accurately described. Never before has this been achieved for any fluxed melt crystal growth process.

Although the authors have restricted themselves to considering bubble materials in the form of single crystals, again it must be stressed that the amorphous Gd–Co alloys [92, 93] and ternary systems based upon these are also potentially suited to magnetic bubble technology. These materials are crystallographically quite dissimilar to the garnets yet have remarkably similar mag-

netic properties so that much of the bubble physics discussed in this article is relevant to these alloys. A review of the Gd–Co system and its application to bubble domain devices has been given by Chaudhari *et al.* [94]. Finally, it is conceivable that hexagonal ferrites [95], spinel ferrites [96]. or some other magnetic material could be developed as epitaxial crystal films to rival garnets.

Acknowledgements

The authors would like to acknowledge many helpful discussions which G. S. Almasi, Y. S. Lin, A. P. Malozemoff, J. C. Slonczewski and numerous other people working in the field of magnetic bubbles. The careful and expert experimental techniques of C. F. Guerci have brought us many useful results. One of us, J. E. Davies, would like to thank IBM World Trade and IBM-U.K. for their support of his Postdoctoral Fellowship.

References

1. P. WEISS, *J. Phys.* **6** (1907) 667.
2. A. H. BOBECK, *Bell Syst. Tech. J.* **46** (1967) 1901.
3. A. H. BOBECK and H. E. D. SCOVIL, *Sci. Am.* **224** June (1971) 78.
4. A. H. BOBECK, R. F. FISCHER and J. L. SMITH, AIP Conference Proceedings No. 5, Magnetism and Magnetic Materials, edited by C. D. Graham Jun. and J. J. Rhyne (A.I.P., New York, 1972) p. 45.
5. G. S. ALMASI, G. E. KEEFE, Y. S. LIN and D. A. THOMPSON, *J. Appl. Phys.* **42** (1971) 1268.
6. H. CHANG, J. FOX, D. LU and L. L. ROSIER, *IEEE Trans. Mag.* **MAG-8** (1972) 214.
7. J. L. ARCHER, L. TOCCI, P. K. GEORGE and T. T. CHEN, *ibid* **MAG-8** (1972) 695.
8. L. J. BOSCH, R. A. DOWNING, G. E. KEEFE, L. L. ROSIER and K. D. TERLEP, *ibid* **MAG-9** (1973) 481.
9. A. A. THIELE, *Bell Syst. Tech. J.* **48** (1969) 3287.
10. *Idem, J. Appl. Phys.* **41** (1970) 1139.
11. D. TREVES, *ibid* **36** (1965) 1033.
12. A. H. BOBECK, R. F. FISCHER, A. J. PERNESKI, J. P. REMEIKA and L. G. VAN UITERT, *IEEE Trans. Mag.* **MAG-5** (1969) 544.
13. A. J. PERNESKI, *ibid* **MAG-5** (1969) 554.
14. E. M. GYORGY, J. P. REMEIKA and F. B. HAGEDORN, *J. Appl. Phys.* **39** (1968) 1369.
15. R. C. SHERWOOD, L. G. VAN UITERT, R. WOLFE and R. C. LECRAW, *Phys. Letters* **25A** (1967) 297.
16. F. ROSSOL, *IEEE Trans. Mag.* **MAG-5** (1969) 562.
17. M. ROBBINS, R. D. PIERCE and R. WOLFE, *J. Appl. Phys.* **42** (1971) 1563.
18. P. BRAUN, *Philips Res. Rep.* **6** (1957) 491.
19. C. KOOY and U. ENZ, *ibid* **15** (1960) 7.
20. L. G. VAN UITERT, D. H. SMITH, W. A. BONNER, W. H. GRODKIEWICZ and G. J. ZYDZIK, *Mat. Res. Bull.* **5** (1970) 455.
21. A. H. BOBECK, *IEEE Trans. Mag.* **MAG-6** (1970) 445.
22. E. F. BERTAUT and F. FORRAT, *Compt. Rend.* **242** (1956) 382.
23. S. GELLER and M. A. GILLEO, *Acta Cryst.* **10** (1957) 239.
24. A. H. BOBECK, E. G. SPENCER, L. G. VAN UITERT, S. C. ABRAHAMS, R. L. BARNS, W. H. GRODKIEWICZ, R. C. SHERWOOD, P. H. SCHMIDT, D. H. SMITH and E. M. WALTERS, *Appl. Phys. Letters* **17** (1970) 131.
25. R. C. LINARES, *J. Crystal Growth* **3/4** (1968) 443.
26. B. COCKAYNE, J. M. ROSLINGTON and A. W. VERE, *J. Mater. Sci.* **8** (1973) 382.
27. B. COCKAYNE and J. M. ROSLINGTON, *ibid* **8** (1973) 601.
28. G. A. KEIG, AIP Conference Proceedings No. 10, Magnetism and Magnetic Materials, edited by C. D. Graham Jun. and J. J. Rhyne (A.I.P., New York, 1973) p. 237.
29. C. D. BRANDLE, D. C. MILLER and J. W. NIELSEN, *J. Crystal Growth* **12** (1972) 195.
30. D. F. O'KANE, V. SADAGOPAN, E. A. GIESS and E. MENDEL, *J. Electrochem. Soc.* **120** (1973) 1272.
31. J. E. MEE, G. R. PULLIAM, J. L. ARCHER and P. J. BESSER, *IEEE Trans. Mag.* **MAG-5** (1969) 717.
32. B. F. STEIN, *J. Appl. Phys.* **41** (1970) 1262.
33. M. ROBINSON, *J. Crystal Growth* **18** (1973) 143.
34. C. W. WILKINS, *ibid* **20** (1973) 207.
35. R. C. TAYLOR and V. SADAGOPAN, *Appl. Phys. Letters* **19** (1971) 361.
36. M. E. COWHER, T. O. SEDGWICK and J. LANDERMANN, *J. Electronic Mats.* **3** (1974) 621.
37. E. D. KOLB and R. A. LAUDISE, *J. Appl. Phys.* **42** (1971) 1552.
38. B. FERRAND, J. DAVAL and J. C. JOUBERT, *J. Crystal Growth* **17** (1972) 312.
39. B. FERRAND, J. GREYNET, D. CHALLETON, J. DAVAL and J. C. JOUBERT, *Mat. Res. Bull.* **9** (1974) 495.
40. H. J. LEVINSTEIN, S. LICHT, R. W. LANDORF and S. L. BLANK, *Appl. Phys. Letters* **19** (1971) 486.
41. E. A. GIESS, J. D. KUPTSIS and E..A. D. WHITE, *J. Crystal Growth* **16** (1972) 36.
42. W. TOLKSDORF, G. BARTELS, G. P. ESPINOSA, P. HOLST, D. MATEIKA and F. WELZ, *ibid* **17** (1972) 322.
43. L. K. SHICK, J. W. NIELSEN, A. H. BOBECK, A. J. KURTZIG, P. MICHAELIS and J. P. REEKSTIN, *Appl. Phys. Letters* **18** (1971) 89.
44. R. HISKES and R. A. BURMEISTER, as [28] p. 304.
45. Y. SUEMUNE and N. INOUE, *J. Crystal Growth* **24/25** (1974) 646.
46. J. E. DAVIES and E. A. D. WHITE, *J. Mater. Sci.* **9** (1974) 1374.
47. S. L. BLANK and J. W. NIELSEN, *J. Crystal Growth* **17** (1972) 302.
48. J. M. ROBERTSON, M. J. G. VAN HOUT, J. C. VERPLANKE and J. C. BRICE, *Mat. Res. Bull* **9** (1974) 555.

49. S. L. BLANK, B. S. HEWITT, L. K. SHICK and J. W. NIELSEN, as [28] p. 256.
50. E. A. GIESS and R. GHEZ, in "Epitaxial Growth", edited by J. W. Matthews (Academic Press, New York, 1975).
51. R..WOLFE, J. C. NORTH, W. A. JOHNSON, R. R. SPIWAK, L. J. VARNERIN and R. F. FISHER, as [28] p. 339.
52. G. S. ALMASI, E. A. GIESS, R. J. HENDEL, G. E. KEEFE, Y. S. LIN and M. SLUSARCZUK, AIP Conference Proceedings No. 24, Magnetism and Magnetic Materials, edited by C. D. Graham Jun., G. H. Lander and J. J. Rhyne (A.I.P., New York, 1975) p. 630.
53. O. VOEGLI, B. A. CALHOUN, L. L. ROSIER and J. C. SLONCZEWSKI, *ibid*, p. 617.
54. E. A. GIESS, B. E. ARGYLE, D. C. CRONEMEYER, E. KLOKHOLM, T. R. MCGUIRE, D. F. O'KANE, T. S. PLASKETT and V. SADAGOPAN, as [4] p. 110.
55. T. MIYADAI, *J. Phys. Soc. Japan* **15** (1960) 2205; **17** (1962) 1899.
56. S. IIDA, *ibid* **22** (1967) 1201.
57. R. F. PEARSON, *J. Appl. Phys.* **33** (1962) 1236.
58. L. G. VAN UITERT, E. M. GYORGY, W. A. BONNER, W. H. GRODKIEWICZ, E. J. HEILNER and G. J. ZYDZIK, *Mat. Res. Bull* **6** (1971) 1185.
59. R. PAUTHENET, *Ann. Phys.* **3** (1958) 424.
60. S. GELLER, J. P. REMEIKA, R..C. SHERWOOD, H. J. WILLIAMS and G. P. ESPINOSA, *Phys. Rev.* **137** (1965) 1034.
61. G. P. ESPINOSA, *J. Chem. Phys.* **37** (1962) 2344.
62. G. P. VELLA-COLEIRO, as [28] p. 424.
63. E. A. GIESS, B. E. ARGYLE, B. A. CALHOUN, D. C. CRONEMEYER, E. KLOKHOLM, T. R. MCGUIRE and T. S. PLASKETT, *Mat. Res. Bull* **6** (1971) 1141.
64. A. ROSENCWAIG and W. J. TABOR, as [4] p. 57.
65. E. M. GYORGY, M. D. STURGE, L. G. VAN UITERT, L. G. HEILNER and W. H. GRODKIEWICZ, *J. Appl. Phys.* **44** (1973) 438.
66. A. AKSELRAD and H. CALLEN, *Appl. Phys. Letters* **19** (1971) 464.
67. W. T. STACY and C. J. M. ROOYMANS, *Solid State Commun* **9** (1971) 2005.
68. T. S. PLASKETT, E. KLOKHOLM and D. C. CRONEMEYER, AIP Conference Proceedings No. 18, Magnetism and Magnetic Materials, edited by C. D. Graham Jun. and J. J. Rhyne (A.I.P., New York 1974) p. 75.
69. E. A. GIESS and D. C. CRONEMEYER, *Appl. Phys.* **22** (1973) 601.
70. J. W. NIELSEN, S. L. BLANK, D. H. SMITH, G. P. VELLA-COLEIRO, F. B. HAGEDORN, R. L. BARNS and W. A. BIOLSI, *J. Electronic Mats.* **3** (1974) 693.
71. R. HISKES, Contract No. DAAH01-72-C-0996, Semi-annual Technical Report, January 1973.
72. J. W. MOODY, R. W. SHAW, R. M. SANDFORT and R. L. STERMER, *Mat. Res. Bull* **9** (1974) 527.
73. W. J. TABOR, G. P. VELLA-COLEIRO, F. B. HAGEDORN and L. G. VAN UITERT, *J. Appl. Phys.* **45** (1974) 3617.
74. W. A. BONNER, J. E. GEUSIC, D. H. SMITH, L. G. VAN UITERT and G. P. VELLA-COLEIRO, *Mat. Res. Bull* **8** (1973) 1223.
75. J. E. DAVIES, E. A. GIESS and J. D. KUPTSIS, *J. Mater. Sci.* **10** (1975) 589.
76. J. C. SLONCZEWSKI, *J. Appl. Phys.* **44** (1973) 1759.
77. F. B. HAGEDORN, *ibid* **45** (1974) 3129.
78. R. C. LECRAW, J. P. REMEIKA and H. MATTHEWS, *J. Appl. Phys.* **36** (1965) 901.
79. R. C. LECRAW, S. L. BLANK and G. P. VELLA-COLEIRO, *Appl. Phys. Letters* **26** (1975) 402.
80. W..J. TABOR, A. H. BOBECK, G. P. VELLA-COLEIRO and A. ROSENCWAIG, *Bell Syst. Tech. J.* **51** (1972) 1427.
81. A. P. MALOZEMOFF, *Appl. Phys. Letters* **21** (1972) 149.
82. T. L. HSU, as [52] p. 624.
83. A. H. BOBECK, S. L. BLANK and H. J. LEVINSTEIN, *Bell Tech. J.* **51** (1972) 1431.
84. R. WOLFE, J. C. NORTH, R. L. BARNS, M. ROBINSON and H. J. LEVINSTEIN, *Appl. Phys. Letters* **19** (1971) 298.
85. R. WOLFE and J. C. NORTH, *Bell Syst. Tech. J.* **51** (1972) 1436.
86. T. H. P. CHANG, *IEEE Trans. Mag.* **MAG-10** (1974) 883.
87. H. I. SMITH, D. L. SPEARS and S. E. BERNACKI, *J. Vac. Sci. Tech.* **10** (1973) 913.
88. E. A. GIESS, J. E. DAVIES, C. F. GUERCI and H. L. HU, *Mat. Res. Bull.* **10** (1975) 355.
89. E. A. GIESS, C. F. GUERCI, J. D. KUPTSIS and H. L. HU, *ibid* **8** (1973) 1061.
90. T. S. PLASKETT, E. KOLKHOLM, D. C. CRONEMEYER, P. C. YIN and S. E. BLUM, *Appl. Phys. Letters* **25** (1974) 357.
91. H. L. HU and E. A. GIESS, as [52] p. 605.
92. P. CHAUDHARI, J. J. CUOMO and R. J. GAMBINO, *Appl. Phys. Letters* **22** (1973) 337.
93. P. CHAUDHARI, J. J. CUOMO and R. J. GAMBINO, *IBM J. Res. Devel.* **17** (1973) 66.
94. P. CHAUDHARI, J. J. CUOMO, R. J. GAMBINO and E. A. GIESS, in "Physics of Thin Films", edited by R. W. Hoffman, Vol. 8 (Academic Press, New York, 1975).
95. P. J. GRUNDY and S. R. HERD, *Phys. Stat. Sol. (a)* **20** (1973) 295.
96. D. A. HERMAN Jun., R. L. WHITE, R. S. FEIGELSON, B. L. MATTES and H. W. SWARTS, as [52] p. 580.

Received 7 April and accepted 14 May 1975.